An Improved Method to Detect Shoreline Changes in Small-Scale Beaches Using Google Earth Pro

T. W. S. Warnasuriya, M. P. Kumara, S. S. Gunasekara, K. Gunaalan & R. M. R. M. Jayathilaka

Taylor & Francis
Taylor & Francis Group

Check for updates

NOTE

An Improved Method to Detect Shoreline Changes in Small-Scale Beaches Using Google Earth Pro

T. W. S. Warnasuriya[a] (iD), M. P. Kumara[a] (iD), S. S. Gunasekara[b] (iD), K. Gunaalan[c] (iD), and R. M. R. M. Jayathilaka[b]

[a]Faculty of Fisheries and Ocean Sciences, Ocean University of Sri Lanka, Tangalle, Sri Lanka; [b]National Aquatic Resources Research and Development Agency, Colombo, Sri Lanka; [c]Department of Fisheries Science, Faculty of Science, University of Jaffna, Jaffna, Sri Lanka

ABSTRACT

Shoreline change studies in small-scale beaches require high-resolution satellite images. In this regard, high-resolution satellite images from Google Earth (GE) would be an alternative source however novel studies are needed to verify the effectiveness and the efficiency of applying those images for shoreline change detection in small-scale beaches. Addressing this gap, the current study attempts to develop a new method. Accuracies of delineated shorelines under different scenarios were used to develop relationships with digitizing methods and used eye-altitude to estimate the most effective, efficient and productive method. This was done using Digital Shoreline Analysis System (DSAS) in ArcGIS software. It was found that the eye-altitude influences on digitizing accuracy and it could be improved when increasing the zoom level of the image which is under investigation. Maximum zoom level (50 m) used in this study showed the highest accuracy in shoreline digitizing while the most productive eye-altitude for shoreline delineation was found as 300 m. The current study identified that GE coupled with DSAS tool in ArcGIS software can be used as an effective and efficient method for small-scale shoreline change analysis and it is suggested that this methodology could be adopted for other similar studies.

Introduction

Shoreline changes are caused by individual or combined effects of natural processes and anthropogenic activities. Such natural processes include wave actions, water currents, tides, winds, sea level rise, storms and tsunami (Ali and Narayana 2015; Dayananda 1992; Pajak and Leatherman 2002) whereas construction of harbours, sand mining, and sand nourishments are among some of such major anthropogenic activities (Oyedotun, Ruiz-Luna, and Navarro-Hernández 2018; Li, Ma, and Di 2002).

CONTACT T. W. S. Warnasuriya ✉ sameethw@ocu.ac.lk; sameethocg@gmail.com 🖅 Faculty of Fisheries and Ocean Sciences, Ocean University of Sri Lanka, Tangalle, 82200, Sri Lanka
This article has been republished with minor changes. These changes do not impact the academic content of the article.

The shoreline is a highly dynamic (Li, Liu, and Felus 2001) boundary that separates land from water (Boak and Turner 2005), and shoreline changes occur as short (Ali and Narayana 2015) or long term (Fenster, Dolan, and Morton 2001) scenarios. Consequences of long term shoreline changes could lead to erosion or accretion (Dayananda 1992). But the trends of erosion or accretion for a given time period cannot be predicted well if they have been caused by extreme events like storms (Dayananda 1992; Dolan, Fenster, and Holme 1991; Fenster, Dolan, and Morton 2001; Forbes et al. 2004). Coastal erosion causes negative impacts on habitats, biodiversity, space, infrastructure and services, public access, recreation, subsistence and cultural practices, and other economic activities. Assessing shoreline changes provides significant insights to coastal impact assessments, risk and decision making in coastal zone management practices (Boateng, Wiafe, and Jayson-Quashigah 2017; Chen et al. 2005; Green et al. 2000). Continuous monitoring of the shoreline through field surveys is more reliable; however, this approach is practically difficult because it is time consuming, labour intensive and expensive. Further, there are large gaps of historic shoreline field data for most parts of the world (Flanders 2013). Therefore, using of remote sensing data in estimating shoreline changes has become very effective and popular (Elnabwy et al. 2020; Warnasuriya, Gunaalan, and Gunasekara 2018).

Aerial photographs from aircrafts or UAVs (Unmanned Aerial Vehicles) (Crommelinck et al. 2016; Paravolidakis et al. 2016), satellite images (White and El Asmar 1999; Zhao et al. 2008), LiDAR (Light Detection and Ranging) data (Hapke et al. 2011; Liu, Sherman, and Gu 2007; White and Wang 2003) and SAR (Synthetic Aperture Radar) data (Lee and Jurkevich 1990; Robinson 2011; Shu, Li, and Gomes 2010; Wang and Liu 2019) are some of the prominent remote sensing data currently used in estimating and monitoring shoreline changes. Aerial photographs and LiDAR data have limited global coverage, and may be obtainable only after necessary approvals and security clearances, which make them less accessible for many regional researchers in the world. As an alternative, some satellite images are now available in the internet for free use. Such satellite imageries include Landsat satellite images from the longest earth observing satellite mission since 1972, and Sentinel satellite images since 2014 which have higher global coverage. Irrespective of the type of satellite images used, the level of accuracy in terms of spatial resolution and georeferencing has become one of the key concerns in current shoreline change detection studies (Amaro et al. 2015; Genz et al. 2007; Guariglia et al. 2006; Li et al. 2008). The required accuracy level depends upon several factors such as, objective and extent of the study, geomorphological features due to dynamic nature of the coast and availability of good quality data. High-

resolution satellite images are well demanded by researchers because of its high accuracy (Bertacchini and Capra 2010; Li, Di, and Ma 2003). For change detection, time series data are needed, however obtaining high-resolution satellite images for different time periods can be expensive and is restricted to available time periods. Interestingly, Google Earth (GE) platform freely offers some high-resolution images for certain years. Therefore, using of GE in scientific studies (Malarvizhi, Kumar, and Porchelvan 2016; Traganos et al. 2018) has increased recognizing GE as an effective tool in educational and research (Nicholson and Dodsworth 2012; Patterson 2007; Sidhu, Pebesma, and Câmara 2018) over the last decade. Few studies have already used satellite images from GE for shoreline change detection and however this effective and inexpensive study approach still needs more development and validation (Li 2016; Warnasuriya, Gunaalan, and Gunasekara 2018).

It is very important to first identify shoreline positions from the satellite images by visual interpretation governed by spatial, radiometric and spectral characteristics (Reddy 2008). High-resolution images can give enough information on land-water boundary and the adjacent coast. Conversely, the shoreline is not very clear in low resolution images for which, image enhancement techniques may be applied either to single band or multiband to identify geomorphological features. The image enhancement techniques provide spatial, radiometric and spectral enhancements by using contrast enhancement, image filtering, arithmetic operations applied on image bands, colour composites (true and false), edge feature enhancement (Paravolidakis et al. 2016) and pan-sharpening. Image classification methods (Lu and Weng 2007) can be used to separate land from water in order to facilitate demarcation of the shoreline as well as to extract coastal land-use types (Wu and Xu 2018). When the land-water boundary is not sufficiently resolved in the images, some other reference lines such as vegetation line or dry-wet line may be used for better understanding of shoreline changes. However, a single shoreline proxy need to be identified throughout a time series of images to measure shoreline changes. Land-water boundary extracted directly from satellite images can be considered as an "Instantaneous Shoreline" (ISL) as this is a sudden capture at one instant in time (Boak and Turner 2005; Dang et al. 2018; Gens 2010; Li, Ma, and Di 2002). GIS (Geographical Information System) techniques that include manual digitizing method or semi-automated method (Altinuc, Keceli, and Sezer 2014; Shu, Li, and Gomes 2010) can be used to extract the ISL from satellite images. During this digitizing process, there is a possibility to introduce errors due to the aforementioned image resolution limitations coupled with human errors and these errors should be considered during the ISL uncertainty estimation. Geo-referencing, tidal variations and wave

actions are the other sources of errors which also contribute to the uncertainty of the ISL. Therefore, estimation of ISL uncertainty plays an important role when describing the accuracy of shoreline change detection studies (Yao et al. 2015). Wave climate data which has open access nowadays (Luo et al. 2018) also can be coupled with remote sensing and GIS data in order to describe shoreline change uncertainties more thoroughly.

Shoreline change can be described in different ways by using shoreline change statistics such as Net Shoreline Movement (NSM), End Point Rate (EPR), Average Of Rate (AOR), Shoreline Change Envelop (SCE), Weighted Linear Regression Rate (WLR) which help to understand the shoreline change patterns quantitatively and qualitatively (Dolan, Fenster, and Holme 1991). It is very important to use the most appropriate change statistics for a given time series of shoreline positions because some scenarios cannot be explained meaningfully by using certain statistics (Dolan, Fenster, and Holme 1991). Typical example is when the time span between shorelines is very low, the EPR cannot be trusted. Combination of several statistics and use of supplementary statistics can ensure the reliability of the results. Most of the current shoreline change detection studies are based on measuring change in shoreline position along roughly shore-perpendicular measurement transects using the Digital Shoreline Analysis System (DSAS) developed by United States Geological Survey (USGS) to implement shoreline change statistics (Armah 2011; Ahmad and Lakhan 2012; Dewidar and Frihy 2010; Hapke et al. 2011; Himmelstoss 2009; Mahapatra, Ratheesh, and Rajawat 2014; Nassar et al. 2019) while few other studies have focused on area-based shoreline change analysis (Anfuso et al. 2016).

Further, the methods used to delineate and analyze the shorelines are also very crucial as some methods introduce more errors resulting uncertain outcomes (Hapke et al. 2011). Collectively, the published shoreline change estimation studies have focused on global, national or regional changes, with the least attention to detect changes in small-scale beaches (small sandy beaches isolated in local scale extending to a limited extent) of given regions. On the other hand, information derived from medium or low resolution satellite images for lengthy shorelines doesn't reflect the dynamism of small-scale beaches well. Thus, the up to date literature survey indicated the need of GIS studies that would validate the use of GE high-resolution images as effective, efficient and free sources during shoreline change studies in small-scale beaches. Such model studies would also produce more reliable outcomes which could subsequently be applied for other similar studies. Therefore, the main aim of the current study was to address the above study gap along with the objectives of (a) developing a methodology to use GE Pro for shoreline change studies in a selected

small-scale beach and (b) verifying the efficiency and effectiveness of the above method in order to make it validated for future studies.

Study area

Pareiwella Beach site is an isolated sandy beach located in Tangalle, southern Sri Lanka, approximately 200 km away from the capital Colombo (Figure 1a). It is a recreationally important bathing beach sheltered by reefs with some rock outcrops (Rathnayake 2015). This beach is bordered by a breakwater of the Tangalle fishery harbor established in 1964 (Gerritsen and Amarasinghe 1976) at the north end, while there is a natural rocky shore at south. A shore-perpendicular groyne between the middle of the beach and natural rocky area offshore was developed after the 2004 Indian Ocean Tsunami. Due to distribution of natural and artificial barriers, the beach has a convex shape seaward with a salient near the middle of the beach. The Pareiwella Beach lies between 6°1'23.22"N, 80°48'2.80"E to 6° 1'19.51"N, 80°48'1.34"E extending approximately 180 m in length. The adjacent reef is rich in biodiversity consisting of corals, seaweeds, seagrasses and other micro and macro flora and fauna (Gunathilake et al. 2015). Both locals and foreigners frequently visit this site as this is one of the attractive beaches in the down south of Sri Lanka. According to the study carried out by Rathnayake in 2015, the economic benefits of this beach are estimated to be LKR 6.39 million (≈34398.48 USD) per year for locals from visitors. These environmental, economic, social and scientific values have made this small beach a significantly important site in Sri Lanka. Climate of the area belongs to Dry Zone according to the Sri Lankan climatic zones classified based on rainfall and is influenced by southwest and northeast monsoons during June to September and December to March respectively (De Vos et al. 2014). Tidal pattern at the site is semi-diurnal and the tidal range varies between 0.5 m to 0.6 m during Spring Tides and 0.1 m to 0.24 m during Neap Tides (Gerritsen and Amarasinghe 1976; Pattiaratchi and Wijeratne 2009). According to the Sri Lankan coastal wave climate, the study area belongs to the High Energy Zone where the wave height ranges 1.3 m to 3.5 m and 1.1 m to 3 m during the southwest and northeast monsoons respectively (Survey Department of Sri lanka 2007).

Methodology

Data collection

Primary data
Extracted shorelines. On the high-resolution images (0.31–1.84 m) from various satellites in GE Pro platform (Table 1), the land-water
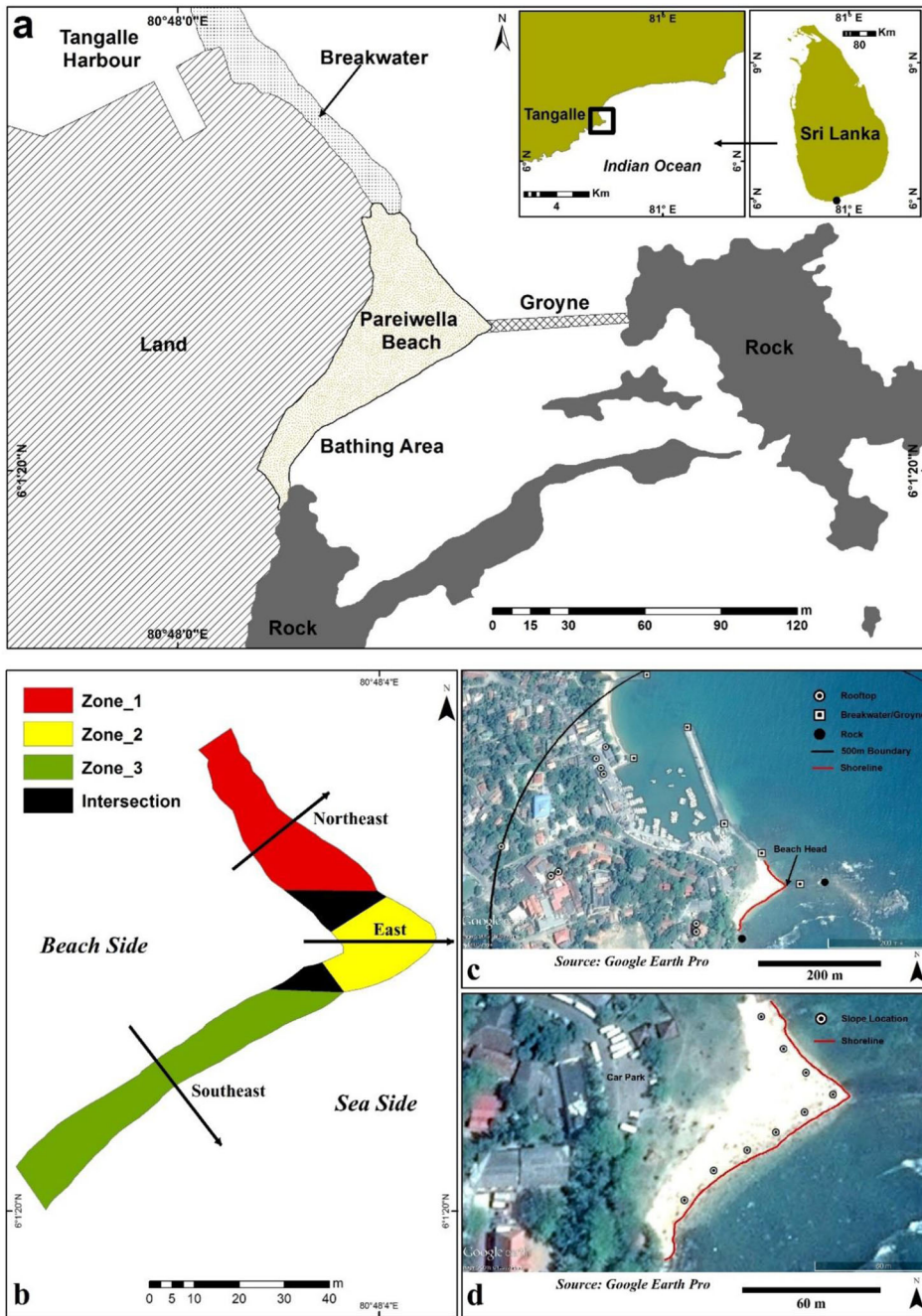
Figure 1. (a) Location map of study area showing Pareiwella beach and adjoining features. Source: T. W. S. Warnasuriya, (b) Zones used for shoreline uncertainty estimation (Note: Depicted Zones have been developed based on the SCE for all the years other than year 2005 because, this is an extreme case which could not be clearly represent in the diagram. Zone overlapping has been mentioned as intersection), (c and d) Ground Control Points (GCPs) of the study site (c – Rooftop, Breakwater, Groyne, Rock, 500 m boundary, Shoreline; d – Slope location, Shoreline).

Table 1. General specifications of the satellite images used in the study.

Date	Monsoon period	Approximate spatial resolution (m)	Approximate radiometric resolution (bits)	Image courtesy
27/09/2003	Southwest	0.65–0.82	11	Digital Globe
28/01/2005	Northeast	0.65–0.82	11	Digital Globe
19/02/2006	Northeast	0.65–0.82	11	Digital Globe
04/07/2009	Southwest	0.46–1.84	11	Digital Globe
08/03/2012	Northeast	0.46–1.84	11	Digital Globe
24/02/2013	Northeast	0.46–1.84	11	Digital Globe
22/02/2014	Northeast	0.5*	12*	CNES/Airbus
14/03/2016	Northeast	0.31–1.84	11	Digital Globe
11/02/2017	Northeast	0.5*	12*	CNES/Airbus

Note: * denotes the confirmed values using the specification of EOS (Earth Observing System) website (Sources: Google Earth Pro, Digital Globe web site, CNES website, EOS website).
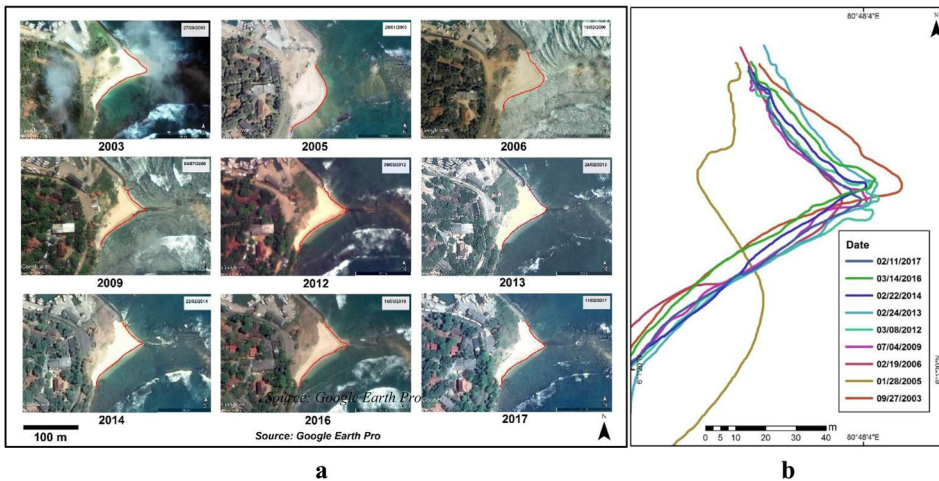
Figure 2. (a) Satellite images from Google Earth for each year for the study site (Pareiwella Beach, Tangalle), (b) Delineated shorelines showing the distribution for different years.

boundary of the study beach site (Pareiwella) was delineated (Figure 2) along the studied shoreline by manual free-hand digitizing method using 'Path' tool for each year (2003 to 2017) at 20 different eye-altitudes ranging from 50 m to 1000 m with an interval of 50 m. Three replicate shorelines were delineated at the same place under each eye-altitude for each year in three different times by a single user. Tilt of the satellite images was kept 0° at each digitizing by activating 'Do not automatically tilt while zooming' option in GE. The time spent for each digitizing process was measured using a stop-watch. This was used to establish relationships between: (a) digitizing time and eye-altitude, (b) normalized digitizing time and eye-altitude and, (c) digitizing speed and eye-altitude separately. Computer specifications were kept constant and the same computer placed in the same environment was used throughout the entire digitizing process.

Table 1explains the specifications of the high-resolution satellite images used in the study. Image courtesy was found from copyright information displayed on Google Earth Pro for respective images. Approximate spatial and radiometric resolutions of the images were estimated based on several factors such as specifications of available high-resolution images in the image source, size of the smallest possible identifiable features from the images and the clarity of the images. Spatial and radiometric resolutions of 2017 and 2014 images were confirmed using the specifications of images which are available for purchase from EOS (*Earth Observing System*) website.

Ground control points (GCPs) and measurements. From GE Pro platform. Nine locations of rooftops laid within 500 m distance from the beach head seen in all the 2003 to 2017 satellite images (Figure 1c) were marked (total 81 place marks) as the point features on the GE Pro platform for each year. All these points were marked under 50 m eye-altitude (eye-altitude at which the features are identifiable under maximum zoom level) and 0° tilt. Geometric measurements (length, width) of objects (such as buildings, breakwaters, groynes, rocks, buses, cars, boats, 3-wheelers) and image shift distance (obtained from the shift of GCPs) with their shift directions were obtained using the ruler of GE Pro. The ground features were verified using GE Street View.

From ground survey. Global Positioning System (GPS) locations of permanent structures adjacent to the beach (buildings, breakwaters, groynes, rocks etc.: Figure 1c) and the locations of beach slope measurements (Figure 1d) were obtained using a "Garmin eTrex 20" hand-held GPS instrument under 4 m accuracy (Garmin Ltd 2020). Geometric measurements (length and width) of the aforementioned structures and vehicles were obtained using a measuring tape in order to interpret the spatial resolution of the satellite images by considering the clarity and visibility of the same features or similar features from the image in terms of their size.

Beach slope. Beach slope was measured for two days in each monsoon period by using a clinometer at nine places (Figure 1d) in the swash zone (three replicates at each place) during the southwest (2018) and northeast (2019) monsoon periods. According to Figure 6, pole 1 was fixed at the land-water boundary during the low tide and pole 2 was fixed in the berm crest. Paired t-test was used to see if there is a significant difference in beach slope between the two monsoon periods. Historical data such as construction activities, beach morphological changes, economic activities, social activities and human alterations were collected via community interviews focusing on local people and related officers.
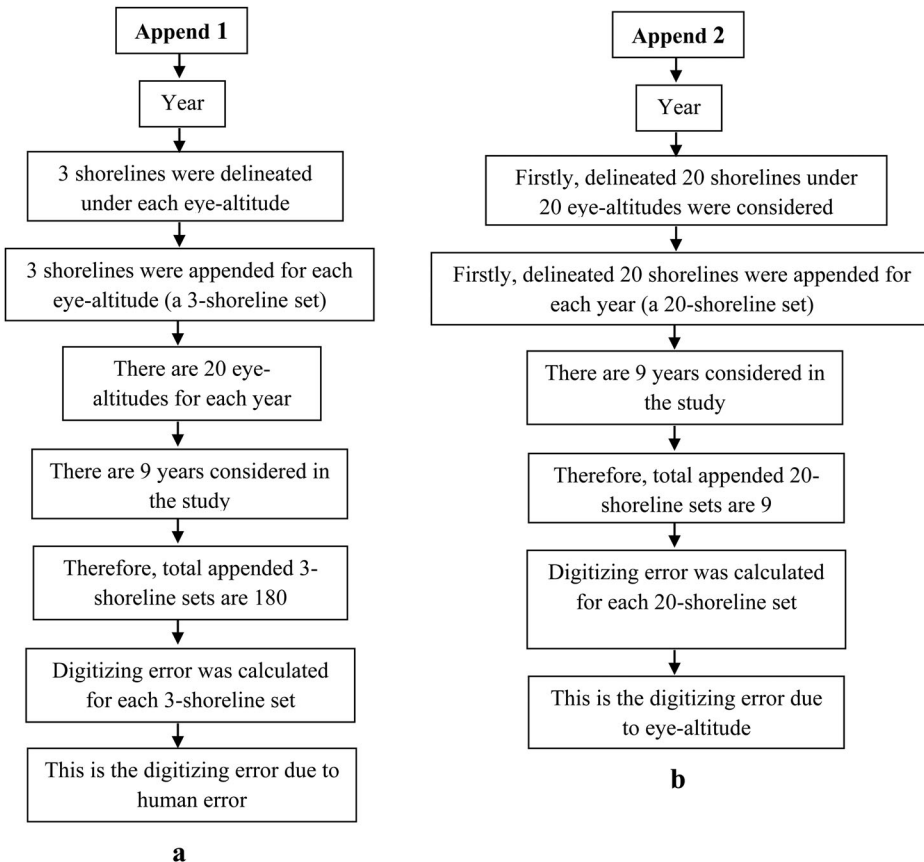
Figure 3. Flow charts of the append scenarios (a – Append 1; b – Append 2).

Secondary data

Survey maps (1:10,000 and 1:50,000), hydrographic charts, published reports of statistics, government web sites, and research papers were used as secondary data sources to understand the present and past situations of the study area.

Data pre-processing and analysis

All the digitized shorelines and GCPs were saved as KML (Keyhole Markup Language) files from GE Pro. All the saved KML files were then converted to Layer file (Shape file format) in ArcGIS 10.5.1 software. The converted layer files were corrected based on the average distance and direction of image shift (which is discussed under error estimation section) and were managed in a personal geodatabase in ArcGIS. All the shorelines were projected in WGS 1984 UTM (Universal Transvers Mercator) projection. Shorelines were appended (This is essential in DSAS for change

Table 2. Shoreline (SL) append scenarios.

Append scenario	Appending process	No. of SLs in a set	No. of appended SL sets	Purpose
Append 1	Three SLs delineated under each eye-altitude were appended for each year. (Figures 3a and 4a–d)	3	180	To estimate the individual digitizing error under each eye-altitude for each year and to build a relationship between eye-altitude and accuracy.
Append 2	All the initially digitized SLs under each eye-altitude were appended for each year. (Figures 3b and 4e,f)	20	9	To estimate the digitizing error due to the eye-altitude for each year.

detection) using 'Append' tool in ArcGIS 10.5.1 in order to facilitate error estimation under scenarios given in Table 2.

Creation of baselines and transects with zonation

Suitable baselines were created manually by considering all the appended shorelines enabling the intersection at almost equal intervals for each error estimation scenario. One-meter interval transects were cast for each baseline using "Smooth Baseline Cast" method (Smoothing Distance is 10 m) from DSAS tool in ArcGIS software as this close transect spacing reflects even slight changes of small beaches. Transect length varied in different append scenarios as this depends upon the width of appended shoreline sets i.e., maximum length of transect in "Append 1 scenario" (Figure 4a–d) and "Append 2 scenario" (Figure 4e,f) was 10 m.

Due to the high heterogeneity of beach geomorphology (Figure 2b) during the study period within the study area, it was divided into three zones (Figure 1b) based on the shoreline aspect (Table 3) and uncertainty was calculated for each zone.

Error estimation

Digitizing error, tidal error and shifting error of the shorelines were estimated using the method described by Warnasuriya, Gunaalan, and Gunasekara (2018) with additional improvements. Introducing two different scenarios (Append 1 and 2) of digitizing error (described in the section "Digitizing error") with eye-altitude and using of wave runup error in the total uncertainty of shorelines were the main improvements.

Digitizing error. Digitizing error was estimated by using the appended sets of shorelines in "Append 1 scenario" (Figure 4a–d) and "Append 2 scenario" (Figure 4e,f) from DSAS tool to analyze shoreline changes and calculate the change statistics (Ali and Narayana 2015; Himmelstoss 2009).
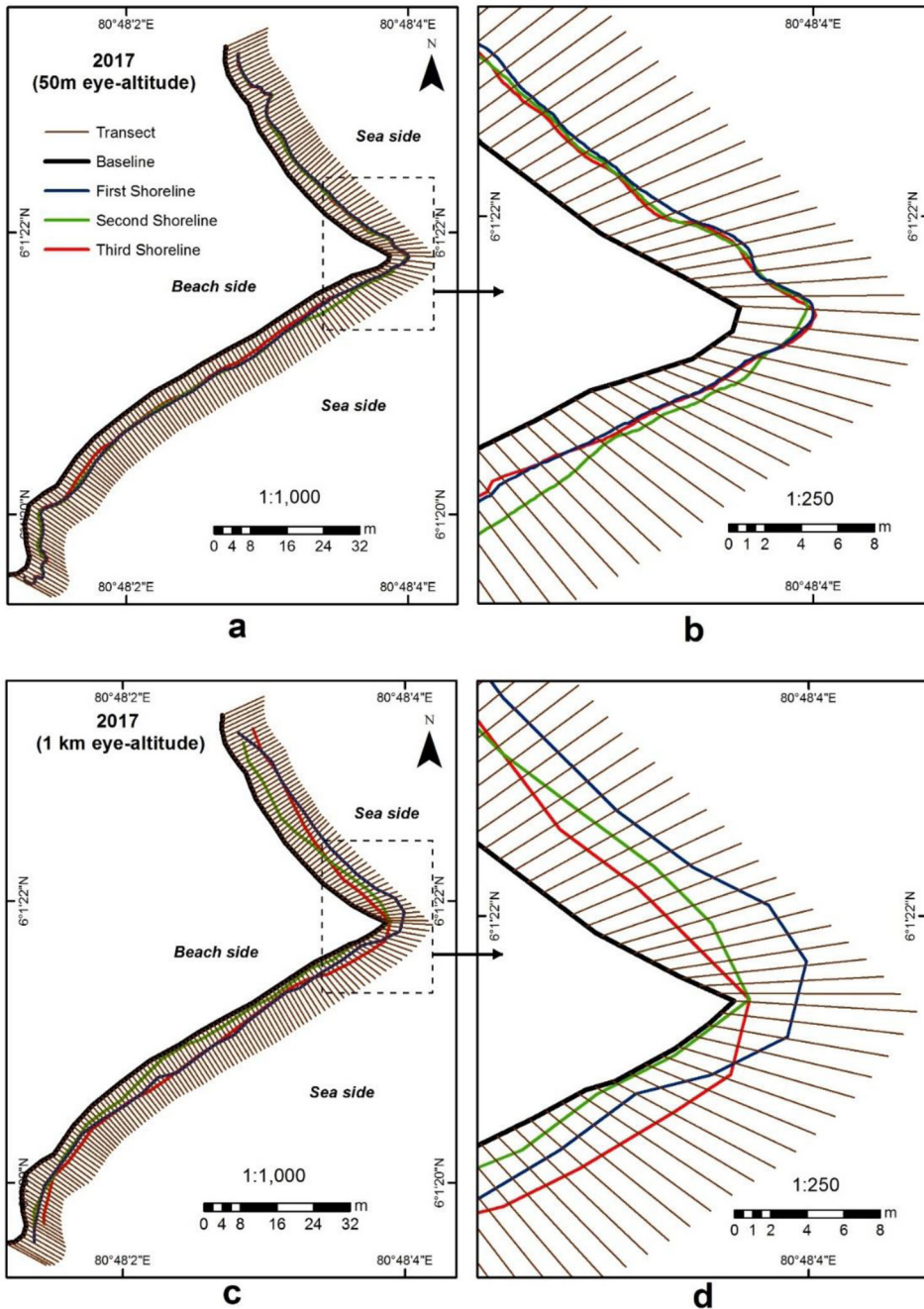
Figure 4. Examples for Append 1 (a–d) and 2 (e, f) Scenarios. (50 m to 1000 m eye-altitudes).

Mock dates (this had to be used because DSAS doesn't work for same dates in the attribute table for shoreline change analysis) were used in "Date_" fields in order to facilitate the error calculation of the shoreline in each year and under different eye- altitudes. This approach was taken as several
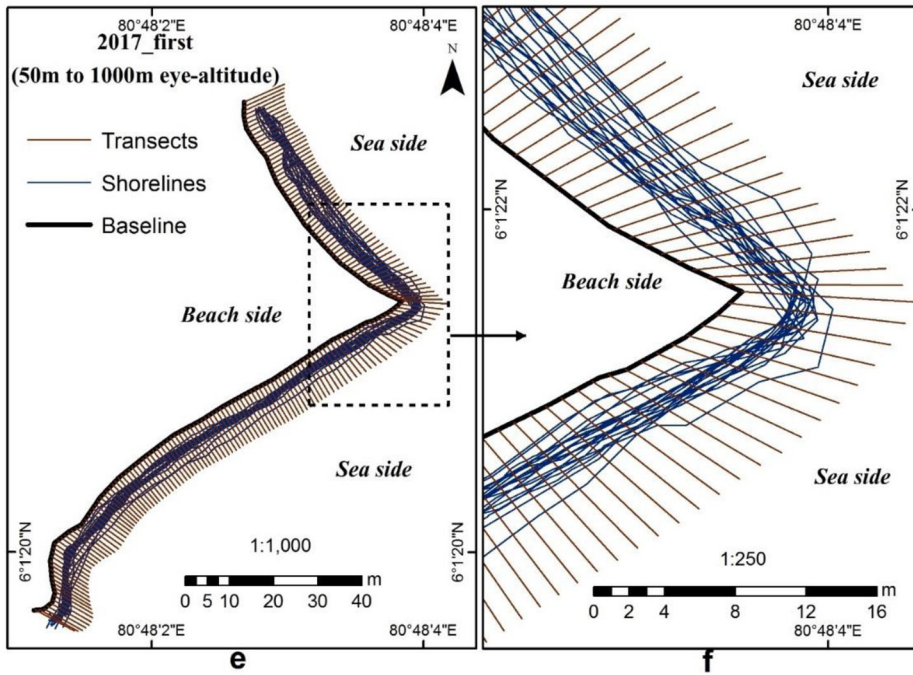
Figure 4. Continued.

Table 3. Shoreline aspect of the beach and coordinate limits in each zone.

Zone	Direction	Start		End	
		Latitude	Longitude	Latitude	Latitude
1	Northeast	6° 1′ 23.498" N	80° 48′ 2.952" E	6° 1′ 22.302" N	80° 48′ 4.036" E
2	East	6° 1′ 22.302" N	80° 48′ 4.036" E	6° 1′ 21.586" N	80° 48′ 3.769" E
3	Southeast	6° 1′ 21.586"	80° 48′ 3.769" E	6° 1′ 20.01" N	80° 48′ 1.616" E

shorelines are used in the calculation for the same date. Gaps between mock dates were kept constant. Shoreline Change Envelope (SCE) was the change statistics used in this regard to estimate the errors as this gives the maximum change of all considered shorelines in the calculation irrespective of the shoreline date. Uncertainty field was not used in the "Append 1 scenario" while the digitizing error estimated from the "Append 1 scenario" was used as the uncertainty of the "Append 2 scenario" in order to estimate the Weighted Linear Regression (WR2) of the error as the uncertainty value is one of the major requirements in this calculation. Average errors under each eye-altitude of all the years were also estimated and the relationship between digitizing error and eye-altitude was established. The trend of the digitizing error due to various shoreline lengths were estimated using the shorelines having 20 m gap between consecutive shorelines along the shore considering all the years. Digitizing error differences between years and between eye-altitudes (One-way ANOVA) and zones (Two-Way
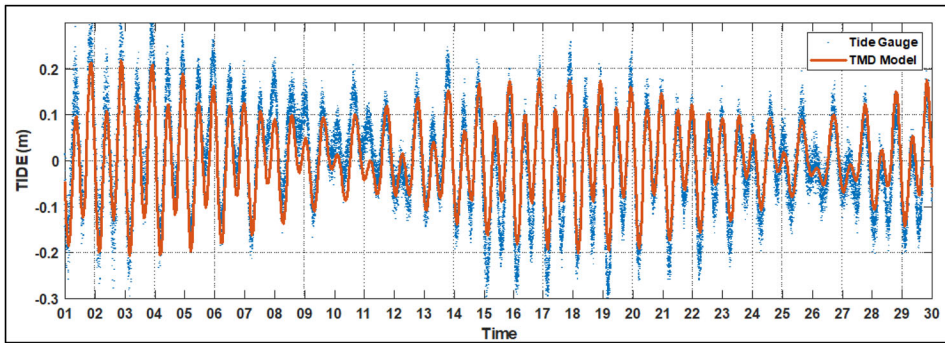
Figure 5. Comparison between measured tide data and TMD model results at Hambanthota fisheries harbor.

ANOVA) were tested. Tukey Post Hoc comparisons were applied wherever necessary for pairwise comparison in different scenarios (e.g., errors between eye altitudes; 50 m and 300 m, 50 m and 1000 m, 300 m and 1000 m). Overall Average Digitizing Error (OADE) for "Append 2 scenario" was calculated by averaging the mean digitizing error of all the years.

Tidal error. Although the tide in Sri Lanka is very small compared to some other parts of the world, this has been taken in to consideration for this study to check the error due to tide with respect to the beach slope and as the guide for other similar studies when apply this method in some other places where the tide is considerable. Horizontal displacement of the shoreline caused by tidal variation was used as the Tidal Error and it was calculated by using approximate tide variation of the study area and its average beach slope. Historical data at the proximity of the study area is not available, therefore global tidal model data were used to estimate the approximate tide. The source for tidal data used in this study is the regional tidal model (TMD) developed by the Oregon State University (Egbert and Erofeeva 2002). TMD was setup for Bay of Bengal at a resolution of 1/ 30 deg. (3.5 km) and the main tidal constituents of M2, S2, N2, K2 and K1 in the study area were extracted. Water level data at Hambanthota tide gauge between 1st and 30th of December in 2009 were used as a validation period for the model. Overall, the model validation shows a moderate performance as shown in the Figure 5.

The main sea level variation in the study area occurs due to the semi diurnal tide (M2) which is considered as the main tidal constituent in Sri Lanka. The spring tide range recorded here is 0.5 m. The extracted main tidal constituents for the study area are listed in Table 4.

Validated tidal model was hindcasted to determine the water level at the time of image acquisition of the shoreline. Image acquisition time was interpreted by considering both shadow evidence (West of the buildings)

Table 4. Extracted main tidal constituents for the study area (regional tidal model).

Tidal constituents	Amplitude (m)	Phase (Degree)
M2	0.1010	265.80
S2	0.0834	294.12
N2	0.0126	271.59
K2	0.0245	292.13
K1	0.0425	273.35
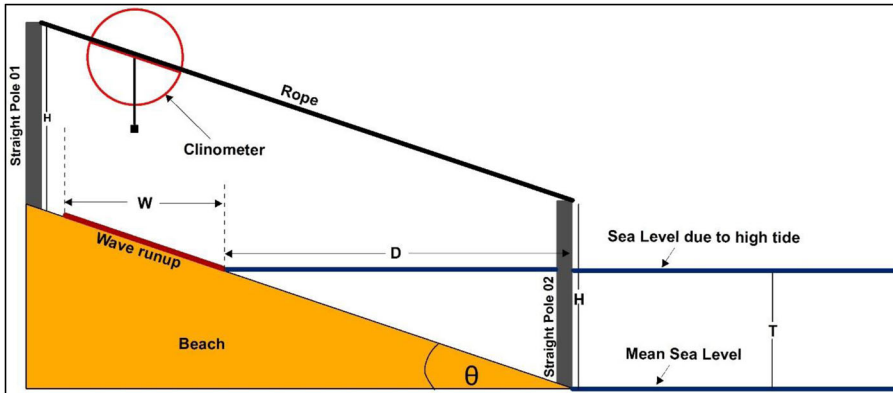
Figure 6. Diagrammatic representation of beach slope analysis, tidal error estimation and wave runup error estimation (not to the scale).

and equator passing time of satellites (10.30 a.m.). Therefore, it was approximated that the images have been obtained around 10.30 a.m.

The average slope of the beach was estimated using a clinometer (Figure 6) and it was used to calculate the tidal error in each zone. The slope data (described in the section "Beach slope") was further used to calculate elevation at each sampling location by using horizontal distance between the locations and Digital Elevation Model (DEM) was created (0.1 m cell size). Shoreline position in 2017 was used as the zero line in the DEM because this is the most recent satellite image used in the study. Beach profiles near the middle of each zone were obtained from the DEM using 3 D Analyst Tool (Profile Graph option) in ArcGIS 10.5.1. It was assumed that the mean slope was not changed during the study period under each monsoon with respect to the past satellite data. Beach slope within monsoons and between monsoons were compared using Paired t test while One-way ANOVA test was used to compare the beach slope in different zones.

Eq. (1) (Warnasuriya, Gunaalan, and Gunasekara 2018) was used to calculate the tidal error (Figure 6). The approximate tide value (Table 5) at the time of image acquisition was used in the equation.

$$\textbf{Tidal error } (\textbf{D}) \ = \ \textbf{Approximate tide value } (\textbf{T})/\textbf{tan } \boldsymbol{\theta} \qquad (1)$$

where, θ = Average beach slope

Table 5. Summary of tide data.

Shoreline date	Most closest moon phase	Day of moon phase	Tide condition	Approximate tide value
27/09/2003	New Moon	26/09/2003	Low	−0.1869
28/01/2005	Full Moon	25/01/2005	Low	−0.2501
19/02/2006	Third Quarter	21/02/2006	Low	−0.1894
04/07/2009	Full Moon	07/07/2009	Flood	0.1101
08/03/2012	Full Moon	08/03/2012	Low	−0.1747
24/02/2013	Full Moon	26/02/2013	Flood	0.0051
22/02/2014	Third Quarter	22/02/2014	Low	−0.1062
14/03/2016	First Quarter	15/03/2016	Low	−0.1747
11/02/2017	Full Moon	11/02/2017	Low	−0.0871

Note: Moon phase was found by Garmin etrex 20 GPS. Tide is given with reference to the Mean Sea Level (MSL).

Shifting error. Some images had shifted compared to the 2017 image and this shift was estimated in terms of the distance and the direction (heading) of the shift. For this purpose, 9 rooftops of the buildings available in all the images within 500 m distance from the beach head were taken into consideration (Figure 1c). Corrections were applied to the shorelines by manual editing based on the shift distance and direction using 'Editor' tool in the GIS software. Standard Deviation (SD) of the shift was used as shifting error of the study.

Wave runup error. Difference between water-land boundary and dry-wet line (W) was used as the wave runup error for each year (Figure 6). Mean SCE in DSAS was used to calculate this difference for each year and each zone under each eye-altitude.

Shoreline uncertainty. The total uncertainty of the shoreline was calculated using Eq. (2) developed by Warnasuriya, Gunaalan, and Gunasekara (2018) by adding newly considered wave runup error;

$$\text{Total Uncertainty} = \text{DE} + \text{TE} + \text{SE} + \text{WE} \qquad (2)$$

where, DE – Digitizing error, TE – Tidal error, SE – Shifting error, WE – Wave runup error

Two-Way ANOVA test was used along with Tukey Post Hoc comparisons to test significant difference of the total uncertainty between different eye-altitudes and zones. Grand mean uncertainty was calculated for maximum possible zoom level (50 m eye-altitude) in order to get an idea about the overall accuracy which could be achieved from the study by averaging the uncertainty in all the years.

Most effective (accurate), most productive and most efficient eye-altitudes were estimated by plotting relationships between (a) digitizing time and eye-altitude, (b) digitizing error and eye-altitude, (c) digitizing error and digitizing time respectively. Differences of the shoreline change statistics between different eye-altitudes and zones were tested by Two-Way
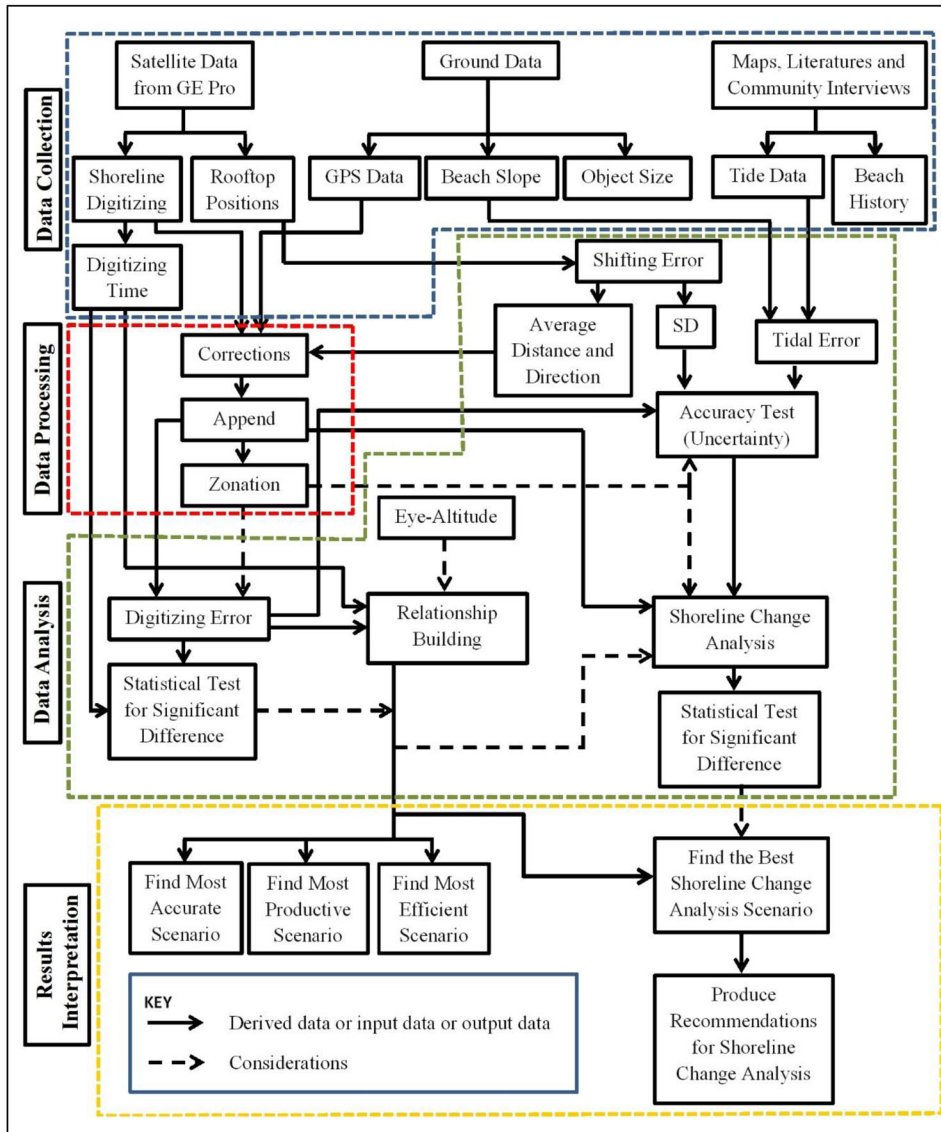
Figure 7. Flow chart showing the overall methodology adopted in this study. Note: Object size was used for spatial resolution interpretation of satellite images. GE stands for Google Earth. GPS stands for Global Positioning System. SD stands for Standard Deviation.

ANOVA test along with Tukey Post Hoc comparisons. Consisted methodology is given in Figure 7.

Eye-altitude responsible for the most productive shoreline was estimated by considering both effectiveness and efficiency. For this purpose, percentage error (Eq. (3)) and percentage digitizing time consumption (Eq. (4)) was calculated and were potted in a graph in order to find the equilibrium point (Figure 10c). Effectiveness and efficiency were calculated using Eqs. (5) and (6), respectively.

$$\text{Percentage error} = (\text{Mean error}/\text{Maximum mean error}) \times 100\% \quad (3)$$

$$\text{Percentage time} = (\text{Mean time}/\text{Maximum mean time}) \times 100\% \quad (4)$$

$$\text{Effectiveness} = 100\% - \%\text{error} \quad (5)$$

$$\text{Efficiency} = 100\% - \%\text{time} \quad (6)$$

The equilibrium point can be considered as the most productive scenario as this contains both high accuracy and high efficiency. Mean productivity was calculated using the Eq. (7).

$$\text{Mean Productivity} = (\text{Effectiveness} + \text{Efficiency})/2 \quad (7)$$

Results and discussions

Relationships between digitizing error and digitizing time with eye-altitude

Under the "Append 1 scenario," the estimated mean digitizing error (mean ± SD) showed its lowest (0.56 ± 0.14 m) and the highest (2.4 ± 0.72 m) values at 50 m and 1000 m eye-altitudes respectively. Minimum and the maximum errors recorded out of all the considered years were 0.39 m and 3.97 m respectively. This type of error can occur due to human errors in digitizing process, reduced image clarity and geomorphology of the beach. Eye-altitude and digitizing error resulted an exponential regression ($R^2 = 0.97$; Figure 8a) where both digitizing error and the standard deviation (SD) of the error exponentially increased with increasing eye-altitude.

Derived equation from this model was;

$$y = 0.5457e^{0.0015x} \quad (8)$$

where, y = Digitizing error (m) and x = Eye-altitude (m)

For direct applications, the equation was linearized and re-written as (Figure 8b);

$$\ln y = 0.0015x + \ln 0.5457 \quad (9)$$

The Figure 8b relationship is useful for researchers to estimate the digitizing error associated with eye-altitude in GE Pro high-resolution images by considering the correction factor of 0.0012 m (slope of the Figure 9) per each exceeding 1 m length of shoreline or vice versa which is described in the Figure 9.

The mean digitizing time (mean ± SD) under each eye-altitude revealed the lowest (9.2 ± 2.59 s) in 1000 m and the highest (64.24 ± 15.43 s) in 50 m. Out of all the considered years, the minimum recorded digitizing time was 6 s while the maximum was 94 s. The trend of mean digitizing time followed a power relationship ($R^2 = 0.99$: Figure 8c) where both digitizing
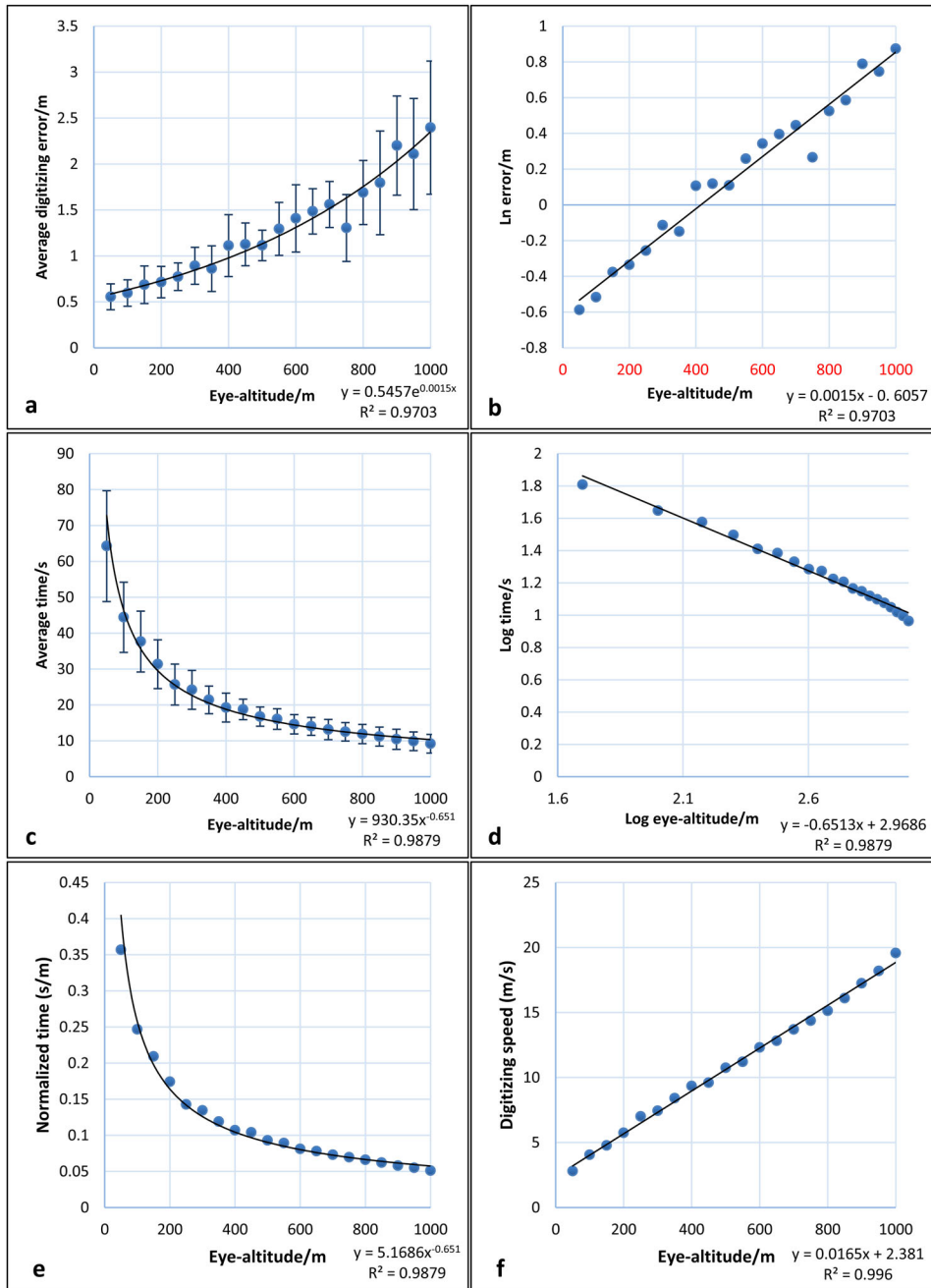
Figure 8. Derived relationships among digitizing error, time and eye-altitude (a – Relationship between eye-altitude and digitizing error, b – Linearized model of the relationship between eye-altitude and digitizing error, c – Relationship between eye-altitude and digitizing time, d – Linearized model for the relationship between eye-altitude and digitizing time, e – Relationship between normalized time and eye-altitude, f – Relationship between average digitizing speed and eye altitude).
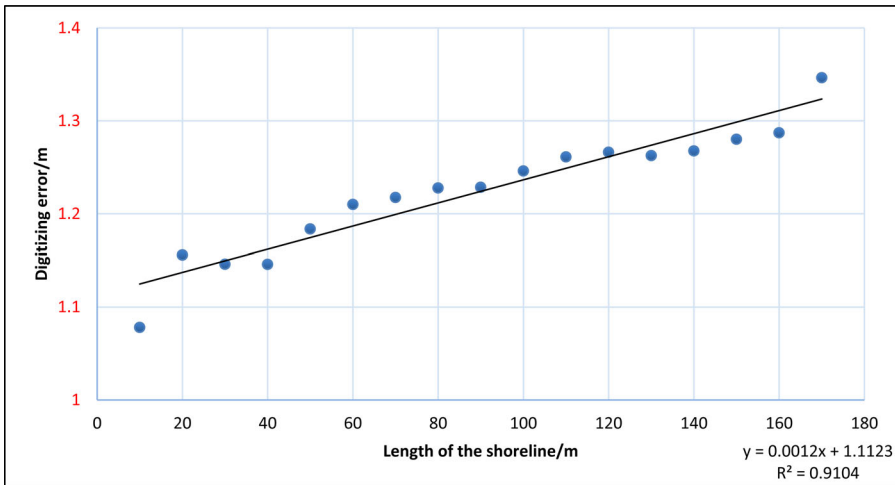
Figure 9. Relationship between shoreline length and digitizing error.

Table 6. Summary of the relationships between percentage digitizing time and percentage digitizing error with respect to eye-altitude.

	Equation	R2	Regression type
Efficiency	$y = 1448.3x^{-0.651}$ (Eq. (14))	0.9879	Power
Effectiveness	$y = 22.772e^{0.0015x}$ (Eq. (15))	0.9703	Exponential

time and the standard deviation (SD) of the digitizing time decreased with increasing eye-altitude.

Derived equation from this model was;

$$\mathbf{y} = 930.35x^{-0.651} \tag{10}$$

where, $y =$ Digitizing time (s) and $x =$ Eye-altitude (m)

For direct applications, the equation was linearized and re-written as (Figure 8d);

$$\log \mathbf{y} = -0.651 \log \mathbf{x} + \log 930.35 \tag{11}$$

The relationship between the eye-altitude and the digitizing time is useful for researchers to estimate the digitizing time associated with eye-altitude in GE Pro high-resolution images. This can be done by considering the curve (Figure 8e) normalized by the shoreline length (180 m) and the derived equation (Eq. (12)) with constant digitizing speed under each eye-altitude. The average digitizing speed for each eye-altitude is given in Figure 8f and it was identified that digitizing speed is linearly increased with increasing eye-altitude.

$$\mathbf{y} = (5.1686x^{-0.651}) * \mathbf{L} \tag{12}$$
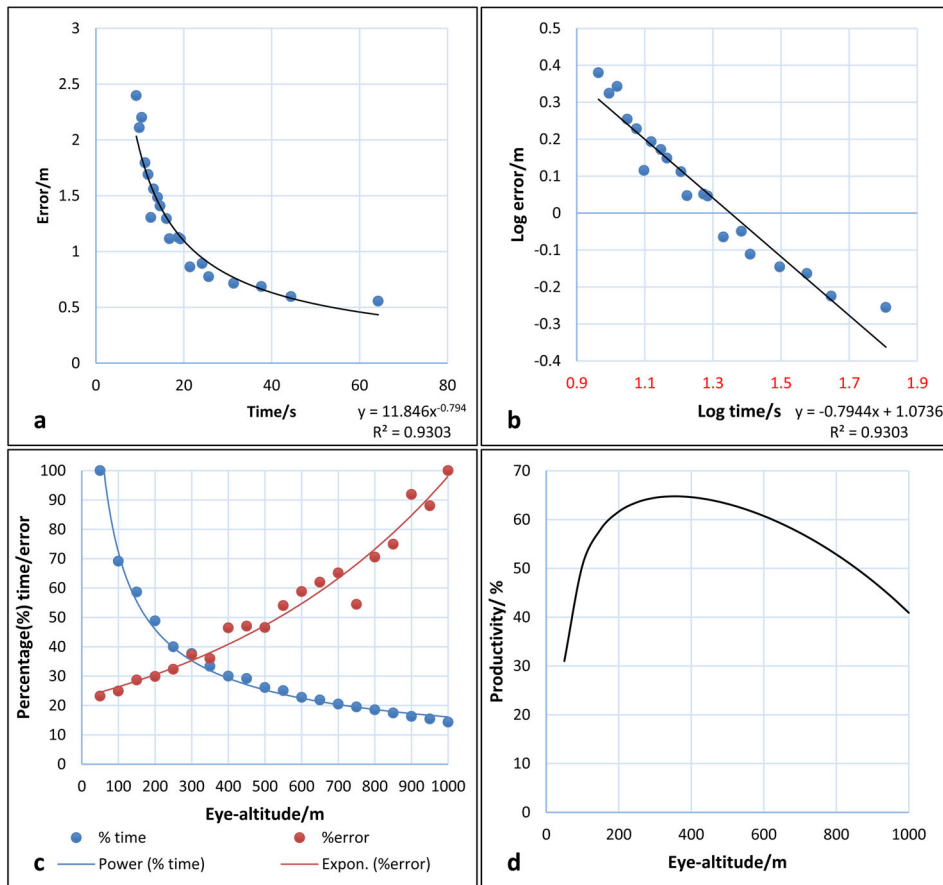
Figure 10. Derived relationships among digitizing efficincy, effectiveness and productivity (a – Relationship between digitizing error and digitizing time, b – Linearized model of the relationship between digitizing error and digitizing time, c – Relationships between percentage digitizing time and percentage digitizing error in association with eye-altitude, d – Productivity curve for shoreline digitizing from high resolution images of GE under different eye-altitudes).

where, y = Normalized digitizing time, x = eye-altitude, L = length of the shoreline in the real world

Relationship between digitizing time and digitizing error (Figure 10a) also followed a power regression model ($R^2 = 0.93$) where the digitizing error decreased with increasing digitizing time.

Derived equation from this model was;

$$y = 11.846x^{-0.794} \tag{13}$$

where, y = Digitizing error (m) and x = Digitizing time (s)

For direct applications, the equation was linearized and re-written as (Figure 10b);

Table 7. Mean productivity of shoreline digitizing under the three eye-altitudes viz. 50 m, 300 m and 1000 m.

	50 m	300 m	1000 m
Efficiency	0	65%	85.68%
Effectiveness	76.82%	65%	0
Mean Productivity	38.41%	65%	42.84%

$$\log y = -0.794 \log x + \log 11.846 \qquad (14)$$

Most accurate (effective), most productive and most efficient eye-altitudes for shoreline change analysis are explained by the graph in Figure 10c. The percentage error followed a power regression model while percentage digitizing time followed an exponential regression model (Figure 10c; Table 6). Time can be considered as an indicator for efficiency and the error can be considered as an indicator for effectiveness where 100% time consumption means low efficiency while 100% error means low effectiveness. In order to become more efficient, digitizing time should be kept low while digitizing error should be kept low for high effectiveness. The study showed the highest effectiveness is at 50 m eye-altitude digitizing while the highest efficiency is at 1000 m eye-altitude digitizing. However, in order to achieve the highest productivity of a digitizing work, both efficiency and the effectiveness should be fulfilled to the highest possible levels.

As the intersecting point (equilibrium point) of the Figure 10c indicates, the highest possible levels of effectiveness and efficiency, the best eye-altitude for shoreline digitizing process from the GE Pro was considered as the eye-altitude at this point where the two curves are intersected. Accordingly, the eye-altitude of this point was 300 m with approximately 35% error and 35% time consumption (Figure 10c). On the other hand, it reveals 65% accuracy and 65% efficiency (Table 7). As this point can fulfill both the highest efficiency and the highest effectiveness, this could be considered as the efficient-effective (e-e) equilibrium of shoreline digitizing which explains the most productive eye-altitude scenario. Therefore, the highest productivity was obtainable at the shorelines from 300 m eye-altitude for a small-scale beach. (Table 7 and Figure10d).

Digitizing error due to "Append 2 scenario" explains the error among 20 eye-altitudes which were taken into consideration in the study (Table 8). One-Way ANOVA showed occurrence of significant error due to "Append 2 scenario" between years ($p < 0.05$) which may be attributed to clarity of the images, slip of the hands during the digitizing process or various geomorphological complexities in different years.

Overall Average Digitizing Error (OADE) due to "Append 2 scenario" was 3.92 ± 0.54 m while the highest (5.00 ± 0.09 m) average error was shown in the year 2003 with the maximum and minimum of 10.04 m and 3.11 m respectively (Table 8; Figure 11). Further, it was identified that the

maximum digitizing error (Append 2) was given in the beach head as shown in the Figure 11. Since no any definite relationship between eye-altitude and the "Append 2" digitizing error (WR2 < 0.5), the resulted digitizing error might be random (Table 9).

The digitizing error (Append 2) depends on digitizing random error and the ability to distinguish water-land boundary under different eye-altitudes. Therefore, for the purpose of change detection, the digitizing should be done under the same eye-altitude for all years through which the digitizing error (Append 2) could be ignored in shoreline uncertainty as there are no any errors introduced due to different eye-altitudes. When different eye-altitudes (between 50 m to 1000 m) are used to delineate the shorelines from GE for different years, this digitizing error (Append 2) should also be taken into consideration during uncertainty calculation. Since our study used the shorelines delineated under the same eye-altitude for change detection at a time, we ignored this digitizing error (Append 2) in uncertainty calculation.

Shoreline uncertainty

In order to calculate the shoreline uncertainty, the tidal error, wave runup error and the shifting error are to be taken into consideration same as the digitizing error mentioned in section "Relationships between digitizing error and digitizing time with eye-altitude." Therefore, under this section the results of digitizing error estimation, tidal error estimation, shifting error estimation, wave runup error estimation and total uncertainty estimation (Table 10) will be discussed under main three different eye-altitude (50 m, 300 m and 1000 m) scenarios and under the three different zones (Zone 1, Zone 2 and Zone 3) of the study area.

Digitizing error

Highest accuracy in terms of digitizing error (0.57 ± 0.12 m) was given in 50 m eye-altitude while the lowest (2.45 ± 0.2 m) of that was given in 1000 m eye-altitude. Mean digitizing error under 300 m eye-altitude was 0.88 ± 0.11 m. Results revealed that it is possible to digitize shorelines under the digitizing error lower than 1 m in both 50 m and 300 m eye-altitudes while the lowest eye-altitude (50 m) can be used to check the results after digitizing. Further, it was identified in certain digitizing under 1000 m eye-altitude could exceed the digitizing error more than 4 m. According to the Two-Way ANOVA test, there was a significant difference in digitizing error among different eye-altitudes ($p < 0.05$). However, Tukey Post Hoc test revealed significant difference in digitizing error neither between 50 m and 300 m eye-altitudes nor between zones ($p > 0.05$). Zone 2 had the highest

Table 8. Digitizing error due to "Append 2 scenario."

	2003	2005	2006	2009	2012	2013	2014	2016	2017
Error/m	5.00	3.74	3.51	3.73	4.53	3.22	3.62	4.02	3.90
SD	0.09	0.22	0.20	0.07	0.23	0.23	0.18	0.21	0.74

Note: SD stands for "Standard Deviation."
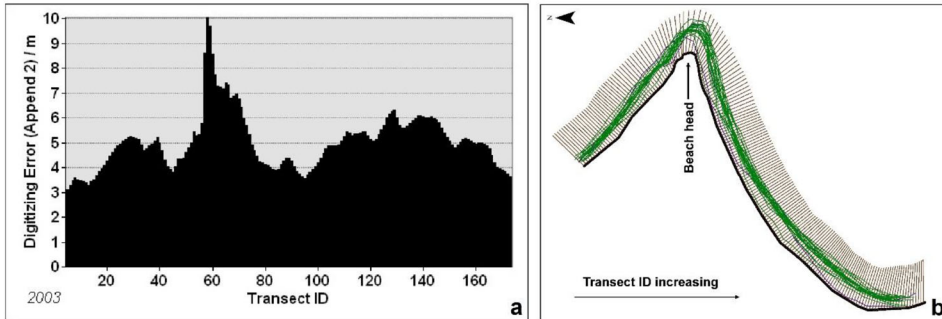
Figure 11. (a) The graph showing the distribution of digitizing error under "Append 2 scenario" (2003) along the baseline under each transect, (b) spatial distribution of digitized shorelines in 2003 under different eye-altitudes and intersected transects.

Table 9. Weighted regression of "Append 2 scenario."

	2003	2005	2006	2009	2012	2013	2014	2016	2017
WR2	0.09	0.08	0.18	0.45	0.26	0.21	0.20	0.35	0.29
SD	0.01	0.04	0.05	0.04	0.02	0.01	0.02	0.09	0.03

mean digitizing error (1.42 ± 0.43 m) compared to other zones. This is due to the complex geomorphology formed by a beach head in this particular zone.

Tidal error

Beach slope and tide at the time of image acquisition were found as the major factors governing the tidal error. The highest mean beach slope ($26.51 \pm 2.29°$) was observed in zone 1 while the lowest ($6.72 \pm 3.46°$) was in zone 2. Further, it was identified that the mean beach slope in southwest monsoon is higher than that of northeast monsoon. None of the three zones showed significantly differed beach slopes ($p > 0.05$: separate paired t-test for each zone) between the two measured days during the northeast monsoon whilst this was significant during the southwest monsoon ($p < 0.05$: separate paired t-test for each zone). For all the three zones, their mean beach slope during the southwest monsoon period was significantly higher ($p < 0.05$: separate paired t-test for each zone) than that of the northeast monsoon period. As the historic ground data for beach slope was not available, it was assumed that the beach slope was not significantly changed in respective monsoon periods of other years. According to the

Table 10. Summary of shoreline uncertainty.

Year	Zone 1			Zone 2			Zone 3		
	50 m	300 m	1000 m	50 m	300 m	1000 m	50 m	300 m	1000 m
2003	15.42	15.81	17.01	19.44	19.42	22.66	5.24	5.76	9.12
2005	12.5	12.83	13.55	15.62	16.02	18.2	8.99	9.11	12.22
2006	8.59	8.96	9.47	14.14	15.08	15.03	10.4	11.06	11.54
2009	6.9	7.21	8.73	12.14	12.46	14.4	6.74	6.92	7.79
2012	4.79	5.19	6.92	14.63	14.8	15.87	8.02	8.18	9.44
2013	6.8	7.09	9.16	10.04	10.31	10.85	5.45	5.77	7.02
2014	5.66	5.91	7.35	5.32	5.53	7.96	3.49	4.07	4.63
2016	6.86	7.0	8.5	12.3	12.47	13.21	5.48	5.99	7.24
2017	4.3	4.65	7.37	9.76	9.8	12.98	5.5	5.34	6.89

two separate one-way ANOVA tests conducted for each monsoon, the beach slope significantly differed ($p < 0.05$) between zones during both northeast and southwest monsoons (Figures 12 and 13).

The highest mean tidal error (1.17 ± 0.61 m) was observed in zone 2 while the lowest (0.35 ± 0.19 m) was in zone 1 which may have been resulted due to differences of beach slope in each zone. The study found that the tidal error is governed by the beach slope (negatively related), monsoon (beach slope is low in northeast monsoon) and the tide at the time the image is acquired. The maximum tidal error (2.12 m) was given in zone 2 of 2005 as it has the highest tidal variation (-0.25 m) and the lowest beach slope ($6.72°$). It was identified that the influence of the tidal error can be kept less than 1 m in the Zone 1 and Zone 3.

Shifting error
The highest image shift (10.67 m) was shown in 2014 image while the highest SD (2.6 m) was shown in 2006 image. SD values of all the other images were lower than 1.5 m. However, the shifting error was assumed to influence all the zones similarly.

Wave runup error
Zone 2 had the highest wave runup error (9.99 ± 3.47 m) while the lowest of that was in zone 3 (4.66 ± 1.6 m). Wave runup error had a greatest contribution to the total uncertainty compared to the other errors. It was found that in some cases this error exceeded more than 10 m across and entire study area.

Total uncertainty
There was a significant difference in shoreline uncertainty among zones and among eye-altitudes (Two-Way ANOVA: $p < 0.05$). However, Tukey Post Hoc test reveals no significant difference in shoreline uncertainty between 50 m and 300 m eye-altitudes ($p > 0.05$). Lowest mean uncertainty
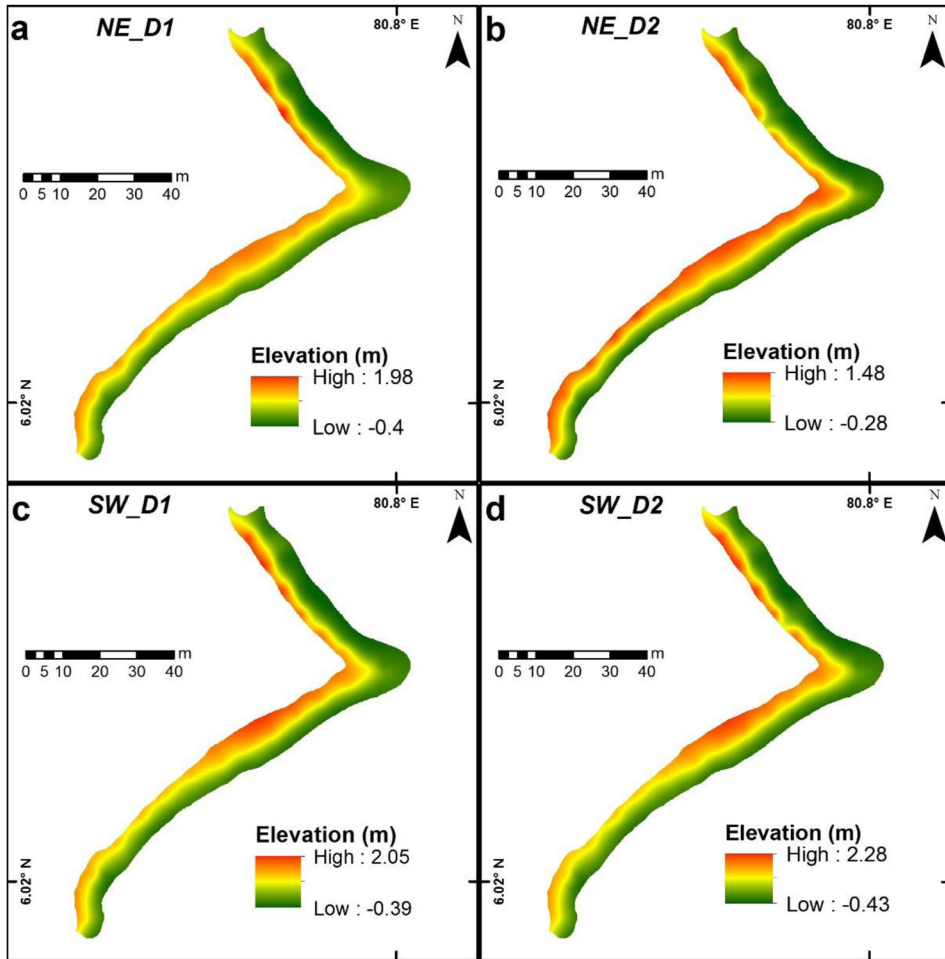
Figure 12. Digital Elevation Models of day 1 (a) and 2 (b) in northeast monsoon, day 1 (c) and day 2 (d) in southwest monsoon.

$(6.59 \pm 2.16\,\text{m})$ was observed in zone 3 under 50 m eye-altitude while highest mean uncertainty $(14.57 \pm 4.22\,\text{m})$ was recorded in zone 2 under 1000 m eye-altitude (Table 10).

Conclusions and recommendations

The current study indicated that the shoreline changes of a small-scale beach can be accurately (Grand mean uncertainty = $9.06 \pm 3.15\,\text{m}$) delineated using images from GE Pro under the eye-altitude (50 m) that has the maximum possible zoom level. However, when considering both effectiveness and efficiency of the shoreline delineation, it was identified that the study had the highest productivity under the eye-altitude 300 m. Although the accuracy is a key factor, efficiency may also be a key
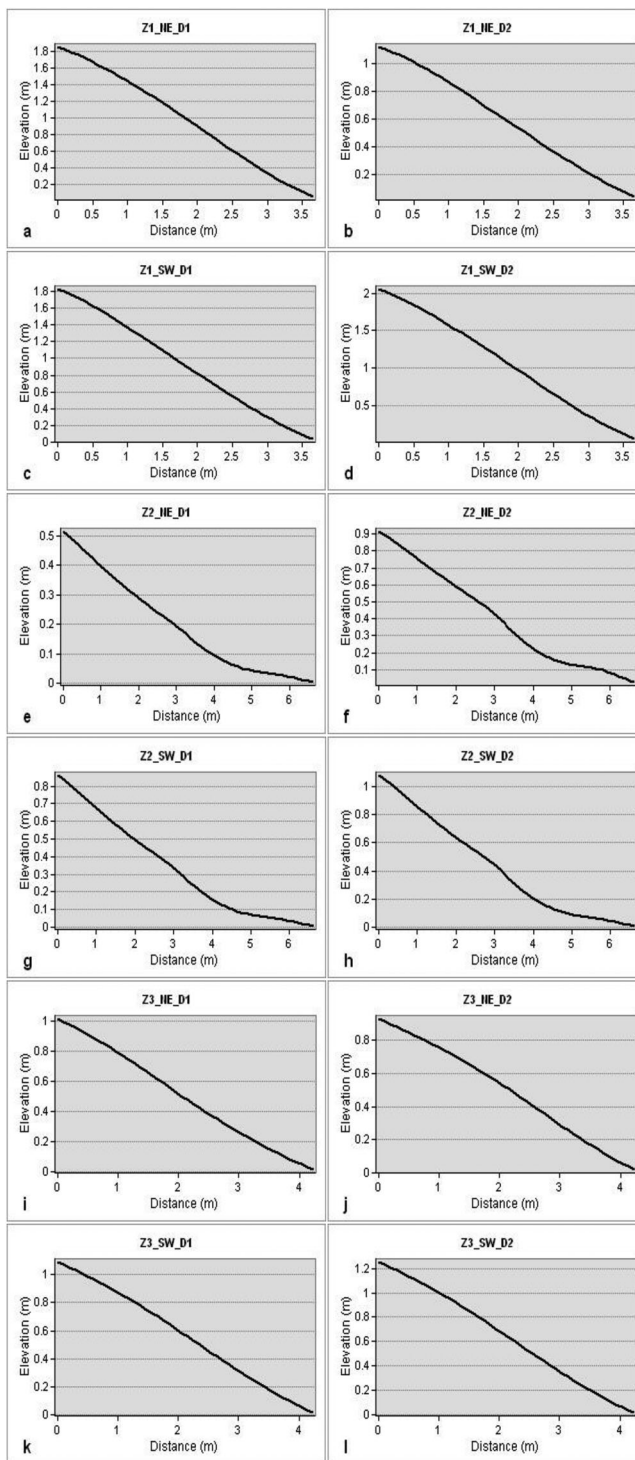
Figure 13. Selected beach profiles from the three zones over two days each of the southwest (SW) and northeast (NE) monsoon (Only middle profiles of each zone are given. Z1 – Zone 1 (a–d), Z2 – Zone 2 (e–h) Z3 – Zone 3 (i–l), D1 – Day 1, D2 – Day 2).

consideration if project duration is limited. In that particular circumstance, minimizing the trade-off between effectiveness and the efficiency is very important. If time is not a concern of the project, 50 m is recommended as the most accurate eye-altitude whilst the most efficient eye-altitude is 1000 m having the highest errors. Further, if there are more shorelines to be delineated or if the shoreline is very long, it is advisable to select the eye-altitude which satisfies both effectiveness and efficiency because; more shorelines or long shoreline consumes much time to delineate and analysis. However, all the shorelines should be delineated under the same eye-altitude in this case. It was identified that DSAS played an important role not only in shoreline change detection but also in shoreline digitizing error estimation as introduced in this study.

The current study indicated that the digitizing error is caused by human errors, image resolution problems and complex coastal morphological features. This error could be minimized by improving the digitizing skills, by correctly identifying the land-water boundary via visual interpretation and selecting the low eye-altitudes for digitizing process. Tidal error was found to be governed by beach slope that significantly changed between the monsoons, tide type (Spring or Neap) and the tide at the time of the image acquisition. However, the tidal errors in this study were low as the tidal variations in Sri Lanka are considered to be very low. The slight image shift found during the study can be corrected in the GIS software. As this shift is not homogenous for all the sampling points, it is ideal to use the SD of the shift as the shifting error in shoreline uncertainty. As the bathing area (Zone 3) of this beach is a pool which is partly covered by reefs and rocks, it could be assumed that the wave action is negligible on this part of the beach leading the lowest uncertainty (6.59 ± 2.16 m). But, in the places where the wave action is high, it is recommended to consider the wave action as one of the error sources (Wave runup error) of the shoreline positions.

The major limitations of the study were (a) temporal gaps in satellite imagery, (b) lack of certain historical ground data for beach slope, winds, waves, tides and currents of the study area, (c) difficulty in finding the exact time of image acquisitions (d) lack of information on exact image resolutions for most of the satellite images and (e) short time span of available imagery only back to the early 2000s, which may not be enough to reliably measure long-term shoreline change trends, especially in an area prone to storm impacts. By considering all the aspects discussed here, it is recommended that the GE Pro can be used as effective and efficient remote sensing and GIS data source for small-scale shoreline change analysis coupled with DSAS tool in ArcGIS software. The methodology followed during the current study could be adopted for other similar small-scale beaches for shoreline change estimations.

Acknowledgements

Authors contribution

Initial concept of the paper came by the first author and he contributed the study by developing the concept and by collecting, processing, analyzing data and interpreting the results including with GIS mapping. Second author supported in the process of statistical analysis, methodology development and concept development along with the results interpretation. Third author supported in the GIS mapping and concept development. Fourth author supported in data analysis and concept development. Fifth author supported in tide data modeling and concept development. All the authors have engaged in article writing by covering various aspects of the study.

Funding

ORCID

T. W. S. Warnasuriya ⓘ http://orcid.org/0000-0001-8074-009X
M. P. Kumara ⓘ http://orcid.org/0000-0001-9192-0387
S. S. Gunasekara ⓘ http://orcid.org/0000-0002-9091-9648
K. Gunaalan ⓘ http://orcid.org/0000-0001-7920-0176

References

Ahmad, S. R., and V. C. Lakhan. 2012. GIS-based analysis and modeling of coastline advance and retreat along the coast of Guyana. *Marine Geodesy* 35 (1):1–15.

Ali, P. Y., and A. C. Narayana. 2015. Short-term morphological and shoreline changes at Trinkat Island, Andaman and Nicobar, India, after the 2004 Tsunami. *Marine Geodesy* 38 (1):26–39.

Altinuc, S. O., A. S. Keceli, and E. A. Sezer. 2014. Semi-automated shoreline extraction in satellite imagery and usage of fractals as performance evaluator. *International Journal of Computer Theory and Engineering* 6 (2):102–6.

Amaro, V. E., L. R. S. Gomes, F. G. F. de Lima, A. C. Scudelari, C. F. Neves, D. V. Busman, and A. L. S. Santos. 2015. Multitemporal analysis of coastal erosion based on multisource satellite images, Ponta Negra Beach, Natal City, Northeastern Brazil. *Marine Geodesy* 38 (1):1–25.

Anfuso, G., D. Bowman, C. Danese, and E. Pranzini. 2016. Transect based analysis versus area based analysis to quantify shoreline displacement: Spatial resolution issues. *Environmental Monitoring and Assessment* 188:1–14.

Armah, F. A. A. 2011. GIS-based Assessment of Short Term Shoreline Changes in the Coastal Erosion-Sensitive Zone of Accra, Ghana. *Research Journal of Environmnetal Sciences* 5:643–54.

Bertacchini, E., and A. Capra. 2010. Map updating and coastline control with very high resolution satellite images: Application to Molise and Puglia coasts (Italy). *Italian Journal of Remote Sensing* 42:103–15.

Boak, E. H., and I. L. Turner. 2005. Shoreline definition and detection: A review. *Journal of Coastal Research* 214:688–703.

Boateng, I., G. Wiafe, and P.-N. Jayson-Quashigah. 2017. Mapping vulnerability and risk of Ghana's coastline to sea level rise. *Marine Geodesy* 40 (1):23–39.

Chen, S., L. Chen, Q. Liu, X. Li, and Q. Tan. 2005. Remote sensing and GIS-based integrated analysis of coastal changes and their environmental impacts in Lingding Bay, Pearl River Estuary, South China. *Ocean & Coastal Management* 48 (1):65–83.

Crommelinck, S., R. Bennett, M. Gerke, F. Nex, M. Y. Yang, and G. Vosselman. 2016. Review of automatic feature extraction from high-resolution optical sensor data for UAV-based cadastral mapping. *Remote Sensing* 8 (8):689.

Dang, Y., C. Zhang, X. Zhou, J. Xu, and S. Xue. 2018. Instantaneous shorelines as an intermediate for island shoreline mapping based on aerial/satellite stereo images. *Marine Geodesy* 41 (3):219–29.

Dayananda, H. V. 1992. *Shoreline Erosion in Sri Lankas's Coastal Areas*. Colombo: Coast Conservation Department of Sri Lanka.

De Vos, A., C. B. Pattiaratchi, and E. M. S. Wijeratne. 2014. Surface circulation and upwelling patterns around Sri Lanka. *Biogeosciences* 11:5909–5930. https://doi.org/10.5194/bg-11-5909-2014.

Dewidar, K. M., and O. E. Frihy. 2010. Automated techniques for quantification of beach change rates using Landsat series along the. *Journal of Oceanography and Marine Science* 1:28–39.

Dolan, R., M. S. Fenster, and S. J. Holme. 1991. Temporal analysis of shoreline recession and accretion. *Journal of Coastal Research* 7:723–44.

Egbert, G. D., and S. Y. Erofeeva. 2002. Efficient inverse modeling of Barotropic ocean tides. *Journal of Atmospheric and Oceanic Technology* 19 (2):183–204.

Elnabwy, M. T., E. Elbeltagi, M. M. El Banna, M. M. Y. Elshikh, I. Motawa, and M. R. Kaloop. 2020. An approach based on landsat images for shoreline monitoring to support integrated coastal management - A case study, ezbet elborg, nile delta. *ISPRS International Journal of Geo-Information* 9 (4):199.

Fenster, M. S., R. Dolan, and R. A. Morton. 2001. Coastal storms and shoreline change: Signal or noise? *Journal of Coastal Research* 17:714–20.

Flanders, D. 2013. *Identifying shoreline changes over time in northern manitoba using historic and current national topographic system maps.* Vancouver, Canada: DPI Territorial Consulting Inc. for Whelan Enns Associates.

Forbes, D. L., G. S. Parkes, G. K. Manson, and L. A. Ketch. 2004. Storms and shoreline retreat in the southern Gulf of St. Lawrence. *Marine Geology* 210 (1-4):169–204.

Garmin Ltd. 2020. *Owner's manual.* eTREX. https://doi.org/10.1016/j.freeradbiomed.2013.07.001

Gens, R. 2010. Remote sensing of coastlines: Detection, extraction and monitoring. *International Journal of Remote Sensing* 31 (7):1819–36.

Genz, A. S., C. H. Fletcher, R. A. Dunn, L. N. Frazer, and J. J. Rooney. 2007. The predictive accuracy of shoreline change rate methods and alongshore beach variation on Maui. *Journal of Coastal Research* 231:87–105.

Gerritsen, F., and S. R. Amarasinghe. 1976. Coastal problems in Sri Lanka. In *Coatal engineering*, 3487–505. Honolulu: American Society of Civil Engineers. https://icce-ojs-tamu. tdl.org/icce/index.php/icce/article/view/1970/1463

Green, E. P., P. J. Mumby, A. J. Edwards, and C. D. Clark. 2000. *Remote sensing handbook for tropical coastal management.* Paris: UNESCO.

Guariglia, A., A. Buonamassa, A. Losurdo, and R. Saladino. 2006. A multisource approach for coastline mapping and identification. *Annales Geophysicae* 49:295–304.

Gunathilake, I. M. I. S. B., I. P. S. C. Halgahawaththa, M. B. M. Fayas, W. A. S. Chamika, and M. F. M. Fairoz. 2015. Present status of Paraviwella Reef Tangalle Southern Sri Lanka: A potential natural mesocosm for marine research. In Proceedings of the First International Symposium on Environmental Management and Planing. Central Environmental Aurhority Sri Lanka, Colombo, 1.

Hapke, C. J., E. A. Himmelstoss, M. G. Kratzmann, J. H. List, and E. R. Thieler. 2011. *National assessment of shoreline change: Historical shoreline change along the New England and Mid-Atlantic Coasts.* Virginia: U.S. Geological Survey Open-File Report 2010 – 1118. https://pubs.usgs.gov/of/2010/1118/pdf/ofr2010-1118_report_508_ rev042312.pdfhttps://pubs.usgs.gov/of/2010/1118/pdf/ofr2010-1118_report_508_ rev042312.pdf

Himmelstoss, E. A. 2009. Dsas 4.0 installation instruction and user guide. In *Digital Shoreline Analysis System (DSAS).* Thieler, E.R., Himmelstoss, E.A., Zichichi, J.L., and Ergul, Ayhan (eds.). U.S. Geological Survey Open-File Report 2008–1278.

Lee, J. S., and I. Jurkevich. 1990. Coastline detection and tracing in SAR images. *IEEE Transactions on Geoscience and Remote Sensing* 28:662–8.

Li, J. 2016. Using Google Earth in the study of shoreline erosion process. ASEE's 123rd Annual Conference & Exposition. American Society of Engineering Education, New Orleans.

Li, R., S. Deshpande, X. Niu, F. Zhou, K. Di, and B. Wu. 2008. Geometric integration of aerial and high-resolution satellite imagery and application in shoreline mapping. *Marine Geodesy* 31 (3):143–59.

Li, R., K. Di, and R. Ma. 2003. 3-D shoreline extraction from IKONOS satellite imagery. *Marine Geodesy* 26 (1-2):107–15.

Li, R., J. K. Liu, and Y. Felus. 2001. Spatial modeling and analysis for shoreline change detection and coastal erosion monitoring. *Marine Geodesy* 24 (1):1–12.

Li, R., R. Ma, and K. Di. 2002. Digital tide-coordinated shoreline. *Marine Geodesy* 25 (1-2): 27–36.

Liu, H., D. Sherman, and S. Gu. 2007. Automated extraction of shorelines from airborne light detection and ranging data and accuracy assessment based on Monte Carlo simulation. *Journal of Coastal Research* 236:1359–69.

Lu, D., and Q. Weng. 2007. A survey of image classification methods and techniques for improving classification performance. *International Journal of Remote Sensing* 28 (5): 823–70.

Luo, Y., D. Wang, T. P. Gamage, F. Zhou, C. M. Widanage, and T. Liu. 2018. Wind and wave dataset for Matara, Sri Lanka. *Earth System Science Data* 10 (1):131–8.

Mahapatra, M., R. Ratheesh, and A. S. Rajawat. 2014. Shoreline change analysis along the coast of South Gujarat, India, using digital shoreline analysis system. *Journal of the Indian Society of Remote Sensing* 42 (4):869–76.

Malarvizhi, K., S. V. Kumar, and P. Porchelvan. 2016. Use of high resolution Google Earth satellite imagery in landuse map preparation for urban related applications. *Procedia Technology* 24:1835–42.

Nassar, K., W. E. Mahmod, H. Fath, A. Masria, K. Nadaoka, and A. Negm. 2019. Shoreline change detection using DSAS technique: Case of North Sinai coast. *Marine Georesources & Geotechnology* 37 (1):81–95.

Nicholson, A., and E. Dodsworth. 2012. Academic uses of Google Earth and Google Maps in a library setting. *Information Technology and Libraries* 31 (2):102–17.

Oyedotun, T. D. T., A. Ruiz-Luna, and A. G. Navarro-Hernández. 2018. Contemporary shoreline changes and consequences at a tropical coastal domain. *Geology, Ecology, and Landscapes* 2 (2):104–14.

Pajak, M. J., and S. Leatherman. 2002. The high water line as shoreline indicator. *Journal of Coastal Research* 18:329–37.

Paravolidakis, V., K. Moirogiorgou, L. Ragia, M. Zervakis, and C. Synolakis. 2016. Coastline extraction from aerial images based on edge detection. *ISPRS Annals of Photogrammetry, Remote Sensing and Spatial Information Sciences* III-8:153–8.

Patterson, T. C. 2007. Google Earth as a (not just) geography education tool. *Journal of Geography* 106 (4):145–52.

Pattiaratchi, C. B., and E. M. S. Wijeratne. 2009. Tide gauge observations of 2004-2007 Indian ocean tsunamis from Sri Lanka and Western Australia. *Pure and Applied Geophysics* 166 (1-2):233–58.

Rathnayake, W. 2015. Should 'Paraviwella Beach' in Sri Lanka be preserved for 'sea bathing'? A ZTCM approach. *Sabaragamuwa University Journal* 14 (2):86–100.

Reddy, M. A. 2008. *Remote sensing and geographical information systems*. 3rd ed. Hyderabad: BS Publications. https://doi.org/10.1017/S0376892900039278

Robinson, D. G. 2011. *Analysis and evaluation in shoreline detection in the South Holland province, using images in quad polarization mode from TerraSAR-X*. University of Twente.

Shu, Y., J. Li, and G. Gomes. 2010. Shoreline extraction from RADARSAT-2 intensity imagery using a narrow band level set segmentation approach. *Marine Geodesy* 33 (2-3): 187–203.

Sidhu, N., E. Pebesma, and G. Câmara. 2018. Using Google Earth Engine to detect land cover change: Singapore as a use case. *European Journal of Remote Sensing* 51 (1): 486–500.

Survey Department of Sri lanka. 2007. *National atlas of Sri Lanka*. 2nd ed. Colombo: Survey Department of Sri Lanka.

Traganos, D., D. Poursanidis, B. Aggarwal, N. Chrysoulakis, and P. Reinartz. 2018. Estimating satellite-derived bathymetry (SDB) with the Google Earth Engine and sentinel-2. *Remote Sensing* 10 (6):859–18.

Wang, D., and X. Liu. 2019. Coastline extraction from SAR images using robust ridge tracing. *Marine Geodesy* 42:286-315.

Warnasuriya, T. W. S., K. Gunaalan, and S. S. Gunasekara. 2018. Google Earth: A new resource for shoreline change estimation—Case Study from Jaffna Peninsula, Sri Lanka. *Marine Geodesy* 41 (6):546–80.

White, K., and H. M. El Asmar. 1999. Monitoring changing position of coastlines using Thematic Mapper imagery, an example from the Nile Delta. *Geomorphology* 29 (1-2): 93–105. (99)00008-2

White, S. A., and Y. Wang. 2003. Utilizing DEMs derived from LIDAR data to analyze morphologic change in the North Carolina coastline. *Remote Sensing of Environment* 85 (1):39–47. (02)00185-2

Wu, D., and H. Xu. 2018. An ecological land cover sampling reclassification model for safety estimation of shoreline systems from a flood defense perspective using optical

satellite remote sensing imaging. *Water (Switzerland)* 10: 285. https://www.mdpi.com/2073-4441/10/3/285/htm

Yao, F., C. E. Parrish, S. Pe'eri, B. R. Calder, and Y. Rzhanov. 2015. Modeling uncertainty in photogrammetry-derived national shoreline. *Marine Geodesy.* 38 (2):128–45.

Zhao, B., H. Guo, Y. Yan, Q. Wang, and B. Li. 2008. A simple waterline approach for tide-lands using multi-temporal satellite images: A case study in the Yangtze Delta. *Estuarine, Coastal and Shelf Science* 77 (1):134–42.